

Spontaneous Discrimination of Polycyclic Aromatic Hydrocarbon (PAH) Enantiomers on a Metal Surface

Gonzalo Otero,^[a] Giulio Biddau,^[b] Taisuke Ozaki,^[c] Berta Gómez-Lor,^[a] Javier Méndez,^[a] Rubén Pérez,^{*[b]} and Jose Angel Martín-Gago^{*[a]}

Stereochemistry is an issue of great relevance in both technological and fundamental disciplines.^[1] For instance, many biological molecules present a characteristic chiral structure, which make them suitable for targeting single-enantiomer drugs. Also of basic importance in the framework of the origin of life, it is accepted that a first enantiomeric selection process took place at some stage on the early Earth and resulted in exclusively L-amino acids being incorporated into the proteins of living beings. In these two examples, the enantiomeric separation is performed either between individual molecules or between a molecule and a surface without the need for clustering enantiomorphic molecular crystals.^[2]

Recently, the role played by the surface in the adsorption of molecular chiral species has been emphasized. For example, it has been shown that amino acids can be enantiospecifically adsorbed at chiral surface sites,^[3a] and that a surface is capable of forming chiral domains from the adsorption of achiral molecules^[1a] or amplifying the separation of enantiomorphous molecular networks.^[4] These examples show the capability of surfaces to provide an effective template for chiral molecular discrimination, with double fundamental

and technological significance. However, in most of the previous studies the molecule–molecule interactions are the cause of chiral recognition. Herein we report on a confined surface-mediated recognition process, in which the local surface–molecule interaction exclusively results in enantiomeric discrimination, and we present large-scale DFT calculations to explain the atomistic mechanism behind the enantiomeric recognition. Thus, we show that thermal under-vacuum deposition on a surface of a three-fold symmetrical polycyclic aromatic hydrocarbon (PAH) leads to adsorption-induced chirality.^[5] This chirality is produced because the molecular landing on the surface could be on one side or the other, which induces a prochiral symmetry break.^[5] We conclusively demonstrate that the surface distinguishes the way in which an individual molecule lands: right- or left-hand adsorbed molecules clearly show different orientations with respect to the underlying substrate. Moreover, we present an atomistic view of the enantiomeric recognition mechanism. We rationalized the interaction of large PAHs on single crystal surfaces and concluded that the final configuration maximizes the favorable adsorption of its constituent benzene-like subunits.

For this study we chose the C₆₀H₃₀ molecule.^[6a] This PAH has acquired a particular relevance after the very recent publication by our group that showed that a surface-catalyzed cyclodehydrogenation process of this planar precursor can transform it into C₆₀ fullerenes.^[6b] A key point for understanding the cyclization mechanism is the interaction of those precursors with the catalytic surface. Figure 1, left, shows a sketch of the molecular geometry of the C₆₀H₃₀ PAH as determined from ab initio calculations. Although the 2D projected molecular form is achiral (Figure 1, left), the free molecule adopts a helical (propeller-shaped) conformation and is, therefore, chiral.^[6b] However, upon adsorption, the molecule planarizes but is still chiral because of the surface and shows different handedness depending on its landing side. Figure 1, center, shows an STM image at the same scale of an individual deposited PAH on Pt(111). This image shows an intensity enhancement in the central part

[a] G. Otero, Dr. B. Gómez-Lor, Dr. J. Méndez, Dr. J. A. Martín-Gago
Structure of Nanoscopic Systems Group
Instituto de Ciencia de Materiales de Madrid
Sor Juana Inés de la Cruz, 3, Cantoblanco, 28049, Madrid (Spain)
Fax: (+34)913729623
E-mail: gago@icmm.csic.es

[b] G. Biddau, Dr. R. Pérez
Departamento de Física Teórica de la Materia Condensada
Universidad Autónoma de Madrid, 28049-Madrid (Spain)
Fax: (+34)914974950
E-mail: ruben.perez@uam.es

[c] Dr. T. Ozaki
Research Center for Integrated Science (Japan)
Advanced Institute of Science and Technology (JAIST)
1-1 Asahidai, Nomi, Ishikawa 923-1292 (Japan)

Supporting information for this article is available on the WWW under <http://dx.doi.org/10.1002/chem.201002079>.

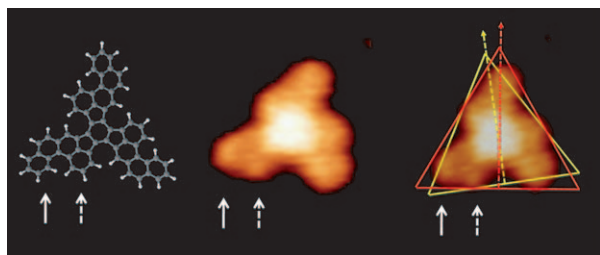


Figure 1. Left: Atomic model of $C_{60}H_{30}$. Center: STM image of $C_{60}H_{30}$. Right: STM image of $C_{60}H_{30}$ circumscribed by a red triangle. The yellow triangle defines the real orientation of the adsorbed molecule with respect to the underlying substrate after calculations (see the Supporting Information for details). Arrows are used to define the molecular chirality.

that covers the central hexagonal ring and the three adjacent pentagons. Figure 1, right, shows the STM image overlaid on the model. It is clear that the outermost aromatic ring in each wing of the molecule is not imaged by the STM. This effect is related to both topography and electronic effects. We have checked that the C atoms located at the peripheral ring present a lower local density of states (see the Supporting Information). The STM image is surrounded by a triangle that can be used to define the overall orientation of the molecule with respect to the surface crystallographic directions (Figure 1, red triangle). Note that this triangle does not correspond with the real molecular orientation but is actually 9° offset in the counter-clockwise direction (Figure 1, yellow triangle).

After submonolayer PAH deposition at room temperature, many triangular shaped features, corresponding to individual molecules, are observed scattered over the surface (Figure 2). They do not form long-range-ordered islands or higher-order superstructures through intermolecular electrostatic interactions as reported for other PAHs.^[4,7] This is an indication of the very small diffusion length at room temperature and shows that the interaction of the molecule with the substrate is high enough to prevent molecular networking. Furthermore, we have not observed any preferential adsorption at step edges, which confirms that the diffusion length should be of the order of the molecular size. A closer look at the molecules (Figure 2, inset) reveals that STM is able to resolve the internal structure and identify the landing orientation: we found molecules with the wings oriented to the left (as in Figure 1) or upside-down (right configuration). As expected, we found a racemic mixture of left and right molecules in a relative statistical proportion of 50% (Figure 2), which confirms that the adsorption process on the surface has the same probability for both molecular faces. As a guide for the eye, we have enclosed in red (white) triangles the molecules exhibiting left configurations (right configurations). We observe that triangles with the same color appear oriented in 60° intervals. Therefore, this PAH, which is inherently achiral in its 2D representation, becomes chiral upon confinement on a surface.^[5]

The experimental ability to simultaneously resolve the landing configuration of the molecule and determine the un-

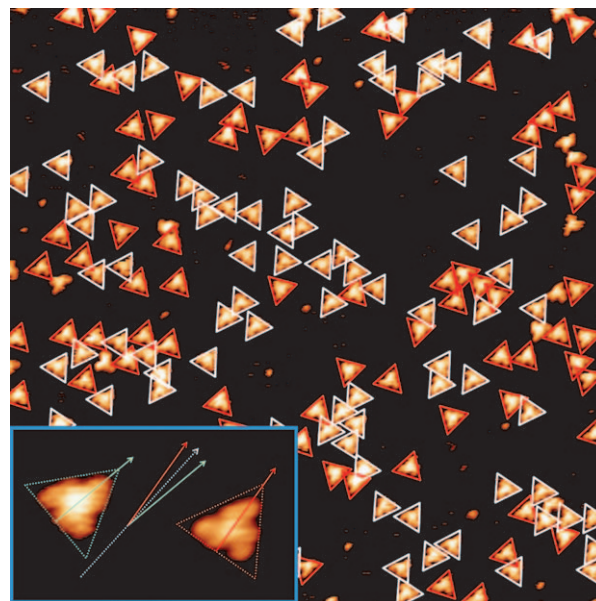


Figure 2. STM image of the $C_{60}H_{30}$ PAHs deposited on a Pt(111) surface. Inset: STM image showing details of two molecules. The white arrow indicates the $[110]$ surface crystallographic direction. Bias voltage and tunnel current are 750 mV and 0.2 nA, respectively.

derlying substrate lattice direction reveals the existence of a marked preferential orientation of the adsorbed PAH molecules with respect to the crystallographic surface directions that correlate with the landing side. The individual molecules point with one axis of the circumscribed triangle $\pm 8^\circ$ off the $[110]$ surface direction (Figure 2, inset). The sign is defined with respect to the counter-clockwise sense. This value has been found by averaging over hundreds of molecules recorded on several days. Therefore, molecules adsorbed with the -8° off orientation have landed in a right configuration, whereas left-configuration molecules adsorb $+8^\circ$ off. However, the real molecular position differs by 9° from the STM image (Figure 1, right), which indicates a total experimental angular separation of every enantiomer and the $[110]$ direction of 17° . The total standard deviation of these values is less than 6° , which shows a very strong and selective correlation between the orientation and the landing side (see the Supporting Information for details of angular determination). The experimentally determined final separation between the two enantiomers is, therefore, about 34° . Our results show that the angular distribution repeats every 60° , which is the symmetry of the outermost layer of the substrate (see Figure 3). This indicates a six-fold symmetry instead of the three-fold symmetry expected for a fcc crystal and it suggests, therefore, the absence of a significant difference between the hollow sites due to the fcc stacking of the crystal surface. Moreover, we have not observed changes in the molecular shape of the STM images induced by the bias voltage.

The preferential orientation of the adsorbed molecules has been studied mainly in enantiomorphous domains of racemic molecules. For instance, molecular networks of hep-

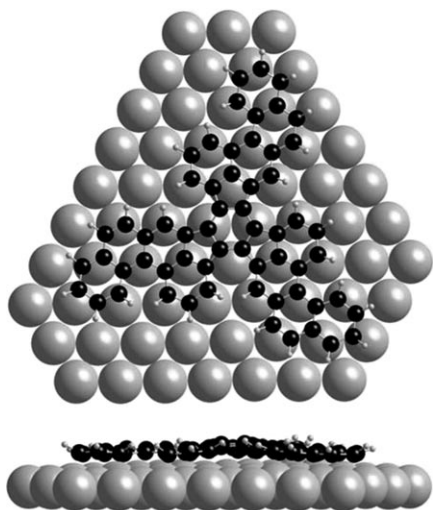


Figure 3. DFT-optimized model of the ground state for the adsorption of $C_{60}H_{30}$ on Pt(111) in a left configuration. The height of a hypothetical circumscribed triangle forms an angle of 18° with the $[\bar{1}10]$ crystallographic surface direction. Note that the wings are locked in a configuration that covers three $[\bar{1}10]$ rows of the substrate.

tahelicene on Cu(111) present a separation of about 10° with respect to the $[\bar{1}10]$ close-packed surface direction.^[4a] This preferential orientation has been attributed to the spontaneous arrangement of the molecules in homochiral domains. However, in our case the adsorbed molecules do not form any higher-order superstructure. Therefore, the separation of 34° between both enantiomers has to be exclusively related to the local surface–molecule interaction. There are other examples of PAH showing selective adsorption,^[3c,d] such as HBC on Au(111), which has been determined to adsorb on fcc stacking regions with a specific orientation of 18° between the molecular axis and the step normal.^[3c]

To understand the highly preferential adsorption orientation and its connection with the landing side, we performed an extensive study using DFT methods to characterize the potential energy surface for one of these large molecules on the Pt(111) surface. OPENMX, a very efficient code based on a local orbital basis, was used to handle these very computationally demanding simulations that involve almost 400 atoms.

The complex phase space for the adsorption has been evaluated with structural optimizations starting from a large set of initial configurations, in which both the position of the central hexagon and the overall orientation of the molecule are varied. In these calculations, all of the atoms in the molecule and those on the two upper Pt layers were allowed to relax. We observe that in several cases the molecule is able to reach a deep ground state through a combination of translation and rotation movements and without an energy barrier, with the molecular wings making an average angle of 18° with respect to the three equivalent $[\bar{1}10]$ surface crystallographic directions (see Figure 3). This is in good agreement with the experiments. In the rest of the configu-

rations, the molecule is trapped in local energy minima that are more than 1.5 eV above the ground energy state.

We have addressed the preferential orientation of the ground-state configuration with a systematic study of the adsorption energy as a function of the angle. Figure 4 summa-

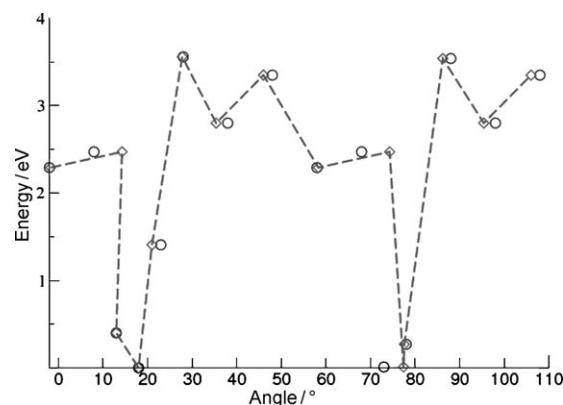


Figure 4. Adsorption energies, referenced to the ground state, as a function of the final angle between the three wings of the adsorbed molecule and the three equivalent $[\bar{1}10]$ surface crystallographic directions, as indicated in the text. The angle for the starting configuration (\circ) and for the final relaxed structure (\diamond) are shown for each calculated clockwise rotation from the ground-state structure, as shown in Figure 3.

rizes the result of our computation by using the same procedure to determine the orientation of the molecules as in the STM images. Our starting structure for these calculations corresponds to a slight translation of the ground state such that the central hexagon occupies a perfectly symmetric bridge position with respect to the underlying Pt lattice. We have considered a number of initial configurations obtained by a rigid clockwise rotation of this structure by an angle in the $[0,120]$ range. All of these configurations have been fully relaxed and the final adsorption energy (taking the ground-state energy as the reference) is displayed in Figure 4 as a function of the final orientation of the molecule. This graph shows two deep minima at $+18^\circ$ and $+78^\circ$ from the $[\bar{1}10]$ direction. They correspond to the ground-state configuration, represented in Figure 3, and another equivalent configuration rotated by 60° , in agreement with the orientations found in the STM images (Figure 2). However, the shape of the energy curve is not perfectly symmetric around the minima. This asymmetry reveals the complexity of the potential energy surface: the relaxation process clearly shows that the molecule exploits both translations and overall rotations in the search for a local energy minimum, and may end up in an angular configuration different from the initial one. Furthermore, the molecule can be trapped in structures with a slightly different rotation for each wing. We have explored the stability of some of these local minima. A very symmetric configuration of the central hexagon seems to be an important limiting step in the relaxation process. Very small displacements of two of the central atoms to break the symmetry are enough to reach the

ground state without any energy barrier. This fact, together with the small energy differences for the intermediate orientations between the two energy minima, indicates that the ground-state configuration can be easily accessed with the thermal energy available during room-temperature deposition. The deep energy minimum around this configuration explains the highly preferential orientation found in the experiments.

Our DFT calculations also support the connection between the landing side and the adsorption orientation. The right-handed molecule, resulting from the prochiral PAH landing on the opposite side, has an adsorption minimum at $+18^\circ$ with respect to the $[\bar{1}10]$ direction. The structure is the mirror reflection of the one shown in Figure 3 and has (within the accuracy of the calculation) the same adsorption energy.

We can rationalize the results discussed above in terms of the energetic for the adsorption of a benzene molecule on the Pt(111) surface. In the ground-state configuration, benzene is located on a bridge site with the C–C bond rotated 30° from the direction of the Pt rows.^[8] Considering the PAH adsorption, the molecule tries to maximize the number of favorable adsorption positions for all of its individual benzene-like rings. There is, however, a competition between the outer hexagons in the wings, which share the same orientation, and the central hexagon, which is rotated by 30° . The former dominate, leading to the ground-state configuration of Figure 3. Other configurations that break this rule are either metastable or have a higher energy. The small difference between the two hollow sites for the adsorption of benzene also explains the approximate 60° symmetry found in our calculations for the molecule-substrate interaction.

The idea that the interaction of the PAHs is controlled by favorable adsorption of the benzene-like subunits also provides a simple explanation for the particular orientation of the adsorbed molecule. The four hexagons in each wing can be accommodated in bridge configurations spanning three atomic $[\bar{1}10]$ rows (see Figure 3 and the Supporting Information). Because the molecule shares a 120° symmetry with the substrate, this can be done simultaneously for the three wings. Assuming this locked configuration and that the rings keep an ideal hexagonal shape, the line joining the center of the central hexagon and the center of the outermost ring in one of the wings makes an angle of 15° with the $[\bar{1}10]$ direction, which is consistent with the angle measured in the experiments. The distortion of those rings in the ground-state configuration explains the deviations from that value in the angles measured in the real structure.

In summary, we present an atomistic view of the surface-molecule interaction responsible for the enantiomeric separation of prochiral PAHs on metal surfaces. In the case of $C_{60}H_{30}$, a precursor for fullerene formation, deposited on a Pt(111) surface, the molecule can settle down in two chiral conformations. Each molecule interacts with the surface to maximize the number of favorable adsorption positions for all the individual benzene-like rings, which leads to a final

configuration rotated by 34° with respect to the opposite chiral form. This mechanism for surface-induced enantiomeric separation could, in principle, operate for any planarized PAH adsorbed on single crystal surfaces.

Experimental Section

$C_{60}H_{30}$ was evaporated in an ultra high vacuum (UHV) environment (base pressure of 2×10^{-10} mbar) and deposited on a clean Pt(111) surface, which was prepared by repeated cycles of sputtering and annealing. The adsorption site and population of the different species was studied by using RT STM images. The images were recorded in topographic mode by using typical values for the tunnel current (0.25 nA) and bias voltages of -2000 , 50 and $50-2000$ mV. Images were analyzed with the WsxM software.^[9]

DFT calculations were performed with the OPENMX^[10] code, which solves the Kohn–Sham equations in a local orbital basis. The wavefunctions are expanded as a linear combination of strictly localized pseudo-atomic orbitals (PAOs) centered on atomic sites.^[11] In these calculations we used a double-zeta basis for H and Pt and 2s and 3p orbitals for C (see the Supporting Information for details). We employed a supercell approach with a three-layer Pt slab with a 10×10 surface periodicity and a vacuum of 9.464 \AA (twice the slab thickness). The molecule is adsorbed only on one side of the slab. The Brillouin zone was sampled with a 221 Monkhorst-Pack mesh. We employed Troullier–Martins pseudopotentials and the LDA approximation for the exchange–correlation functional. Real-space grid techniques with a cutoff energy of 150 Ry were used for the numerical integrations. All of the atoms in the molecule and the Pt atoms in the two upper layers were allowed to relax during the geometry optimization until the forces on each moving atom were $< 0.01 \text{ eV \AA}^{-1}$.

Acknowledgements

Financial support is acknowledged from the projects MAT2008-1497, CSD2007-41, CTQ2007-65683/BQU, S2009/MAT-1756/CAM, MAT2008-02929-NAN, and PLE2009-0061 (MICINN), and by the UAM-Banco Santander Programme for Collaboration with Asia. Computer time was provided by the Cray-XT5 supercomputer at JAIST, the Spanish Supercomputing Network (RES), and by the Centro de Supercomputación y Visualización de Madrid (CeSViMa), which are gratefully acknowledged.

Keywords: chirality • density functional calculations • enantiomeric separation • scanning probe microscopy • surface analysis

- [1] a) M. Linares, A. Minoia, P. Brocorens, D. Beljonne, R. Lazzaroni, *Chem. Soc. Rev.* **2009**, *38*, 806–816; b) D. B. Amabilino in *Chirality at the Nanoscale Nanoparticles, Surfaces, Materials and More*, Wiley-VCH, Weinheim **2009**; c) S. de Feyter, F. C. De Schryver in *Scanning Probe Microscopies: Beyond Imaging* (Ed.: P. Samori), Wiley-VCH, Weinheim, **2006**.
- [2] a) Y. Mastai, *Chem. Soc. Rev.* **2009**, *38*, 772–780; b) W. Xiao, X. Feng, P. Ruffieux, O. Gröning, K. Müllen, R. Fasel, *J. Am. Chem. Soc.* **2008**, *130*, 8910–8912.
- [3] a) A. Kühnle, T. Linderoth, F. Besenbacher, *J. Am. Chem. Soc.* **2006**, *128*, 1076–1077; b) A. Kühnle, T. Linderoth, B. Hammer, F. Besenbacher, *Nature* **2002**, *415*, 891–893; c) P. Ruffieux, K. Palotas, O. Gröning, D. Wasserfallen, K. Müllen, W. A. Hofer, P. Gröning, R. Fasel, *J. Am. Chem. Soc.* **2007**, *129*, 5007–5011; d) M. Böhlinger, K. Morgenstern, W. Schneider, R. Berndt, F. Mauri, A. D. Vita, R. Car, *Phys. Rev. Lett.* **1999**, *83*, 324–324.

- [4] a) R. Fasel, M. Parschau, K. Ernst, *Nature* **2006**, *439*, 449–452; b) B. Xu, C. Tao, W. G. Cullen, J. E. Reutt-Robey, E. D. Williams, *Nano Lett.* **2005**, *5*, 2207–2211.
- [5] a) R. Raval, *Chem. Soc. Rev.* **2009**, *38*, 707–721; b) S. Barlow, R. Raval, *Surf. Sci. Rep.* **2003**, *50*, 201–341.
- [6] a) B. Gómez-Lor, Ó de Frutos, A. M. Echavarren, *Chem. Commun.* **1999**, 2431–2432; b) G. Otero, G. Biddau, C. Sánchez-Sánchez, R. Caillard, M. F. López, C. Rogero, F. J. Palomares, N. Cabello, M. A. Basanta, J. Ortega, J. Méndez, A. M. Echavarren, R. Pérez, B. Gómez-Lor, J. A. Martín-Gago, *Nature* **2008**, *454*, 865–868.
- [7] a) J. Weckesser, A. D. Vita, J. V. Barth, C. Cai, K. Kern, *Phys. Rev. Lett.* **2001**, *87*, 96101–96104; b) P. Ruffieux, O. Groning, R. Fasel, M. Kastler, D. Wasserfallen, K. Mullen, P. Groning, *J. Phys. Chem. B* **2006**, *110*, 11253–11258; c) R. Kelly, W. Xu, M. Lukas, R. Otero, M. Mura, Y. Lee, E. Laegsgaard, I. Stensgaard, L. N. Kantorovich, F. Besenbacher, *Small* **2008**, *4*, 1494–1500; d) M. Blüm, E. Cavar, M. Pivetta, F. Patthey, W. D. Schneider, *Angew. Chem.* **2005**, *117*, 5334–5337; e) L. J. Prins, P. Timmerman, D. N. Reinhoudt, *J. Am. Chem. Soc.* **2001**, *123*, 10153–10163; f) H. Spillmann, A. Dmitriev, N. Lin, P. Messina, J. Barth, K. Kern, *J. Am. Chem. Soc.* **2007**, *129*, 10725–10728.
- [8] C. Morin, D. Simon, P. Sautet, *J. Phys. Chem. B* **2003**, *107*, 2995–3002.
- [9] I. Horcas, R. Fernández, J. M. Gómez-Rodríguez, J. Colchero, J. Gómez-Herrero, A. M. Baro, *Rev. Sci. Instrum.* **2007**, *78*, 013705 1–8.
- [10] The code, OPENMX, pseudoatomic basis functions, and pseudopotentials are available on the website: <http://www.openmx-square.org/>.
- [11] a) T. Ozaki, *Phys. Rev. B* **2003**, *67*, 155108; b) T. Ozaki, H. Kino, *Phys. Rev. B* **2005**, *72*, 045121.

Received: July 21, 2010
Published online: November 23, 2010